# Nanomicelles Potentiate HDAC Inhibitor Efficacy In Vitro.

**Simone Pisano**
Houston Methodist Research Institute https://orcid.org/0000-0002-5412-1241
**Xiong Wang**
Xi'an Jiaotong University
**Yanzhen Hu**
Xi'an Jiaotong University
**Le He**
Xi'an Jiaotong University
**Deyarina Gonzalez**
Swansea University Medical School
**Lewis Francis**
Swansea University Medical School
**Robert Steven Conlan**
Swansea University Medical School
**Chao Li** ( cli12@xjtu.edu.cn )
Xi'an Jiaotong University

**Research**

**Keywords:** Pluronic, Drug delivery, Nanomicelles, Epigenetic drugs, Cancer, SAHA

**Posted Date:** August 3rd, 2020

**DOI:** https://doi.org/10.21203/rs.3.rs-50247/v1



**Version of Record:** A version of this preprint was published on November 25th, 2020. See the published version at https://doi.org/10.1186/s12645-020-00070-8.

# Abstract

**Background.** Amphiphilic block copolymers used as nanomicelle drug carriers can effectively overcome poor drug solubility and specificity issues. Hence, these platforms have a broad applicability in cancer treatment. In this study, Pluronic F127 was used to fabricate nanomicelles containing the histone deacetylase inhibitor SAHA, which has an epigenetic-driven anti-cancer effect in several tumor types. SAHA loaded nanomicelles were prepared using a thin-film drying method and characterized for size, surface charge, drug content and drug release properties. Loaded particles were tested for in vitro activity and their effect on cell-cycle and markers of metastasis.

**Results.** Following detailed particle characterization, cell proliferation experiments demonstrated that SAHA loaded nanomicelles more effectively inhibited the growth of HeLa and MCF-7 cell lines compared with free drug formulations. The 30nm SAHA containing nanoparticles were able to release up to 100% of the encapsulated drug over a 72h time window. Moreover, gene and protein expression analyses suggested that this effect was achieved through the regulation of p21 and p53 expression. SAHA was also shown to upregulate E-cadherin expression, potentially influencing tumor migration and metastasis.

**Conclusions.** This study highlights the opportunity to exploit pluronic-based nanomicelles for the delivery of compounds that regulate epigenetic processes, thus inhibiting cancer development and progression.



# Funding Information

This study received financial support from the Jiangsu Nature Science Foundation, BK20191188; the Life Sciences Research Network Wales project grant ‘Nanoparticle delivery of epigenetic modifiers: a targeted approach for Endometrial Cancer treatment’; the joint PhD program Swansea University and Houston Methodist.


# 1. Background

Metastasis remains a major clinical challenge in cancer treatment. In this multi-step process tumor cells migrate from primary tumors to distal sites. Cancer cells have the inherent ability to detach from the primary tumor site, invade the extracellular matrix, infiltrate lymphatic or blood vessels, disseminate and eventually form a secondary tumor [1]. One of the mechanisms by which tumor cells acquire metastatic features is through undergoing an epithelial-to-mesenchymal transition (EMT), a cellular process characterized by the loss of epithelial markers (such as E-cadherins) and the overexpression of mesenchymal markers (mainly N-cadherins), which leads to the more aggressive behavior of these cells [2]. E-cadherin and N-cadherin are important members of the cadherin family, which are $Ca^{2+}$ dependent cell adhesion glycoproteins [3]. Cadherins were initially identified in epithelial tissues [4, 5], but subsequent studies found that both proteins were also expressed in cancer cells including Hela and MCF-7. During tumor metastasis, downregulation of E-cadherin is involved in the loss of adhesion of epithelial

cells, and is followed by the increased expression of N-cadherin which provides cells with the characteristics of mesenchymal cells and the ability to invade and metastasize to secondary sites [7, 8].

Chemical compounds directly targeting epigenetic processes have emerged as potential treatments for metastatic disease [9]. Epigenetics involve alterations to the DNA and chromatin landscape and consequently gene expression patterns and biological processes [10]. The molecular alterations to the nucleosome-forming histone proteins is one of the major epigenetic modifications that have been found to be altered in cancer [11]. Compounds targeting these modifications, reverting them to a non-cancer state, have great therapeutic potential. Suberoylanilide Hydroxamic Acid (SAHA, commercially known as Vorinostat) is approved by the FDA for the treatment of malignant cutaneous T-cell lymphoma (CTCL) [12]. Subsequently, it was found to offer therapeutic potential for other cancer types including cervical, breast and prostate [13–15]. SAHA is a histone deacetylase (HDAC) inhibitor that can mediate the downregulation of DNA transcription in numerous biological processes [16] including cell growth arrest, activation of the extrinsic and intrinsic apoptotic pathways, autophagic, reactive oxygen species (ROS)-induced cell death and mitotic cell death [17–21]. Furthermore, SAHA appears to inhibit tumor invasion and metastasis, and studies have confirmed that another HDAC inhibitor trichostatin A (TSA) can down-regulate E-cadherin expression [22–24]. Limitations in SAHA utility include low bioavailability, short half-life and toxic side-effects, which are partly linked to the development of multidrug resistance (MDR) [1, 25, 26]. Together, these factors have limited clinical use of SAHA as an effective anticancer treatment [27, 28]. Encapsulating SAHA within nanoparticles represents a potential strategy for overcoming such limitations to enhance its utility in clinic.

Nanoparticles including liposomes [29], bio-nanocapsules [30], polymeric nanoparticles [31], chitosan nanoparticles [32] and polymeric micelles [33] are being developed to overcome poor solubility and drug efficacy [34]. Due to the unique physiological and pathological features of the tumor site, correctly sized nanomicelles can be passively targeted due to the enhanced permeability and retention (EPR) effect, which can improve the drug efficacy and reduce the toxic and side effects of the drug [35–37]. Nanomicelles possess unique advantages including structural stability and simplicity of fabrication in a 10–100 nm size-range [38, 39]. They can also effectively prolong the retention time of drugs *in vivo* and prevent drug inactivation by enzyme degradation before reaching the tumor site [40].

Pluronic is a water-soluble amphiphilic molecule with a poly(oxyethylene)-block-poly (oxypropylene)-block-poly(oxyethylene) (PEOx-PPOy-PEOz) triblock structure [41], which self-assembles forming core-shell micelles in aqueous media. Chlorpromazine (CPZ)-containing Pluronic nanomicelles have been shown to enhance the cytotoxicity of the drug and increase its selectivity towards chronic myeloid leukemia cells, demonstrating the pharmacological potential for cancer treatment [42]. Moreover, Solasodine, a type of steroidal alkaloid that exhibits excellent bioactivities against fungi, viruses, and especially tumors, has been encapsulated into Pluronic F127 nanocarriers, and was able to enhance the anti-cancer effect of Solasodine alone in A549 and Hela cells [43]. A similar approach has also been used for doxorubicin hydrochloride loaded Pluronic F127 nanocapsules which demonstrated delayed drug release[44] .

In this work we demonstrated that SAHA-encapsulated Pluronic nanomicelles are able to efficiently release the drug in a time-dependent fashion and to exert a more cytotoxic effect than the free drug formulation when tested on two breast and cervical cancer cell lines. Moreover, similar to the free drug, the encapsulated SAHA remains effective in triggering cell cycle arrest and apoptosis in a dosage dependent manner. The histone deacetylase inhibitor drug also altered the expression of the EMT markers E-cadherin and N-cadherin suggesting that effective delivery has the potential to reverse the aggressive, metastatic phenotype of these cancer models.

# 2. Methods

### 2.1 Chemicals and reagents

Pluronic F127 was purchased from Sigma, China. SAHA was purchased from Nanjing Duolun Chemical Co., Ltd., China. Acetonitrile, Dimethyl sulfoxide (DMSO), Ammonium persulfate, Sodium chloride, Dodecyl Sodium sulfate, Tween 20, Methanol, Ethanol, Isopropanol and Chloroform were purchased from Sinopharm Chemical Reagent Co., Ltd., China. Phosphate Buffered Saline, Dulbecco's Modified Eagle Medium (DMEM), 1640 Medium, Trypsin were purchased from Solarbio. Fetal Bovine Serum was purchased from Corning. MTT, Glycine, Tris(hydroxymethyl)aminomethane, Acrylamide were purchased from Aladdin, China.

### 2.2 Preparation of SAHA-Pluronic F127 Nanoparticles

200 mg of Pluronic F127 and 3 mg of SAHA were dissolved into 10 ml of acetonitrile. Subsequently, the solvent was removed by rotary evaporation at 55℃ with decompression. The solid copolymer matrix obtained was then preheated at 65℃ for 1 h and eventually hydrated with phosphate buffer solution (PBS, 10mM or 150mM NaCl) or $H_2O$. The nanomicellar solution was filtered with a 0.22 μm filter to remove any free drug. The dispersion, size and zeta potential of nanomicelles was measured by dynamic light scattering (Particle size analyzer, Malvern, UK).

### 2.3 Nanomicelle stability

Nanoparticles were resuspended in either $H_2O$, PBS (10mM NaCl) or PBS (150 mM NaCl) and stored at 4℃. In order to assess the stability of each formulation over time, size and poly-dispersion (PDI) measurements were taken at 0, 5, 10, 15, 20, 25 and 30 days.

### 2.4 Drug release assessment

A high performance liquid chromatography (HPLC) system (Waters 2535, Milford, MA, US) equipped with a photodiode array detector was used for the analysis of the drug release potential of the Pluronic formulations. A C18 HPLC column (GraceSmart RP C18, 4.6 mm × 250 mm, 5 μm) was used for quantitative analysis of SAHA. Mobile phase A contained HPLC grade $H_2O$, and mobile phase B contained HPLC grade acetonitrile. SAHA was eluted with 50% mobile phase A and mobile phase B at a flow rate of

1 ml/min, with a retention time of 3.6 min and UV detection at 265 nm. Standard curves of concentration peaks and areas were drawn. Five-point calibration curves for SAHA in the range of 31.25–500 μM were considered reliable ($r^2 \geq 0.999$).

### 2.5 Determination of drug loading and entrapment efficiency.

200 μl of nanomicelle solution were added with 800 μl acetonitrile and centrifuged for 5 min at 10,225 x g. The supernatant was used to determine the concentration of drug by HPLC.

The entrapment efficiency (EE) and drug loading efficiency (DL) were calculated as follows:

$$DL\% = \frac{\text{Weight of drug in nanomicelles}}{\text{Weight of drug loaded nanomicelles}} * 100\%$$

$$EE\% = \frac{\text{Weight of drug in nanomicelles}}{\text{Weight of drug added into nanomicelles}} * 100\%$$

### 2.6 In vitro drug release

In order to measure the release of SAHA from nanomicelles, a 20 ml solution containing SAHA loaded nanomicelles was loaded into a dialysis bag (MWCO: 8000~14,000 Da, Spectrum®, Rancho Dominquez, CA, USA), which was immersed in 500 ml of 10mM PBS (pH 7.4). Temperature was maintained at 37°C. At predetermined time intervals, 1 mL of release medium (PBS) was withdrawn and replaced with the same volume of fresh PBS into the system. The concentration of SAHA inside the solution was determined by HPLC.

### 2.7 Cell lines

HeLa (human epithelial cervical cancer) and MCF-7 (human breast adenocarcinoma) cell lines were kindly donated by Suzhou Institute of Nano-Tech and Nano-Bionics (SINANO), Chinese Academy of Sciences. HeLa cells were grown in DMEM and MCF-7 cells in RMPI. All media was supplemented with penicillin (100 U/ml) and streptomycin (100 μg/ml) and 10% FBS at 37°C in a humidified 5% $CO_2$ and 95% air atmosphere.

### 2.8 Cell proliferation assay

The anti-proliferative effects of SAHA, SAHA-loaded nanomicelles and empty nanomicelles were assessed using the 3-(4,5-dimethyl-2-thiazolyl)-2,5-diphenyl-2-H-tetrazolium bromide (MTT) assay (Aladdin, China). $1x10^4$cells/well were seeded in 96 well plates, grown overnight, and then treated with various concentrations of SAHA, SAHA loaded nanomicelles and empty nanomicelles for 24 h, 48 h or 72 h. 20 μL of MTT reagent were added to each well and left incubating for 4 hours. The optical density was determined at 490 nm using a Multifunctional Microplate Reader (Thermo Fisher, China).

### 2.9 Western blot

$2.5x10^5$ cells were dispersed in three 6-well plates, grown overnight, and three plates treated with SAHA, SAHA nanomicelles and empty nanomicelles for 24 h or 48 h. The cells were lysed in RIPA lysis buffer containing protease and phosphatase inhibitors (Beyotime, China) and total protein was estimated with BCA Protein Assay Kit (Beyotime, China). Protein was separated by SDS-PAGE and transferred on PVDF membranes (Beyotime, China). The membranes were blocked in 5% skimmed milk, incubated with primary antibodies for p21, p53, N-Cadherin or E-cadherin (Santac Cruz, US), and then incubated with the appropriate HRP conjugated secondary antibody (Absin, China).

### 2.10 Quantitative RT-PCR (qRT-PCR)

Hela and MCF-7 cells were treated with the SAHA and SAHA loaded nanomicelles for 24 h or 48 h. Total RNA was isolated using the RNAiso Plus kit (Takara, Japan). 10ug of total RNA was converted into complementary DNA (cDNA) with PrimeScript RT reagent kit with gDNA Eraser (Takara, Japan). SYBR Premix Ex TaqTM (Takara, Japan) solution was used according to manufacturer's protocol to measure for mRNA expression of p53, p21, E-cadherin and N-cadherin with by qPCR. GAPDH was used as a control to determine relative mRNA expression. The table below shows the primer sequences used.

| Gene | | Primer sequence |
|---|---|---|
| GAPDH | Forward Primer | 5'-GCACCGTCAAGGCTGAGAAC-3' |
| | Reverse Primer | 5'-TGGTGAAGACGCCAGTGGA-3' |
| p21 | Forward Primer | 5'-GATGGAACTTCGACTTTGTCACC-3' |
| | Reverse Primer | 5'-CTGCCTCCTCCCAACTCATC-3' |
| p53 | Forward Primer | 5'-ACTCCCCTGCCCTCAACAA-3' |
| | Reverse Primer | 5'-ATCCAAATACTCCACACGCAAA-3' |
| E-cadherin | Forward Primer | 5'-AGGATGACACCCGGGACAAC-3' |
| | Reverse Primer | 5'-TGCAGCTGGCTCAAGTCAAAG-3' |
| N-cadherin | Forward Primer | 5'-CGAATGGATGAAAGACCCATCC-3' |
| | Reverse Primer | 5'-GCCACTGCCTTCATAGTCAAACACT-3' |

### 2.11 Statistical analysis

Data were expressed as mean ± standard deviation and analyzed using SPSS software. According to the distribution type of the data, the samples were processed by T-test and one-way ANOVA analysis, and $P<0.05$ was considered statistically significant.

## 3. Results

### 3.1 Characterization and assessment of stability of SAHA loaded nanomicelles over time

Nanomicelles were fabricated using a thin film method (see **section 2.2** materials and methods) and characterized by dynamic light scattering. Empty and SAHA loaded nanomicelles both had an average size of 23 nm and a poly-dispersive index (PDI) of 0.09±0.02 and 0.08±0.01 respectively, confirming the uniformity of distribution of the formulation (Table 1). The surface charge of the particles was measured

with the Zetasizer Nano instrument (Malvern, UK), providing a zeta potential value of -1.28±0.28 mV. The entrapment efficiency (EE%) and Drug Loading Efficiency (DL%) values were 94.36±0.76% and 1.31± 0.062%, respectively.

In order to gain more insights into the stability of the nanomicelles, the size of particles in three different solutions ($H_2O$,10mM PBS and 150mM PBS) was measured at different time points for up to 30 days (**Fig. 1**). In all three solvents, the initial particle size of SAHA nanomicelles was 30 nm. In $H_2O$ the micelles aggregated over time, increasing six-fold in size compared to day 0 (**Fig. 1a**). Less aggregation was observed in 10 mM PBS (**Fig. 1b**), and no aggregation was observed for nanomicelles dissolved in PBS containing physiological NaCl concentrations (150mM, **Fig. 1c**). PBS (150mM NaCl) was therefore selected for all further experiments.

### 3.2 Sustained release profiling

SAHA loaded nanomicelles were analyzed for their capacity to sustain SAHA release over time (**Fig. 2)**. SAHA was retained for a longer period of time when loaded in nanomicelles with only 36.53% ±3.43 of drug released after 2 h and 85.68%±2.48 after 72 h, compared to free SAHA where levels reached 51.55% ±1.56 after 2 h, 96.27% ±3.47 after 72 h.

### 3.3 SAHA loaded nanomicelles inhibit Hela cell and MCF-7 cell proliferation

The ability of SAHA loaded nanomicelles to inhibit cell proliferation in both Hela and MCF-7 cancer cell lines was assessed. HeLa and MCF7 cell lines were treated with 1μM and 5μM of free drug or SAHA-encapsulated nanoparticles for up to 72 h. The 1uM concentration of free and encapsulated drug displayed similar toxicities with both Hela and MCF7 cells after 24 h and 48 h (**Fig. 3a, 3c**), while the nanomicelles became significantly more effective than the free drug after 72 h on HeLa cells ($p<0.05$). Conversely, the 5 □M concentration of SAHA-encapsulated nanomicelles proved to be more effective than the free drug after 48 h for both HeLa ($p<0.05$, **Fig. 3b**) and MCF7 ($p<0.01$, **Fig. 3d**). The same trends were maintained after 72 h of exposure to the treatment on both HeLa and MCF7 cells. These observations suggested that nanomicelles encapsulation of SAHA serve to enhance its cytotoxicity.

### 3.4 Effect of SAHA loaded nanomicelles on cell cycle and on EMT.

To evaluate the effect of SAHA encapsulation on the expression of p21 and p53 (cell cycle markers) and on E/N-cadherins (EMT markers), HeLa cells were treated with free and encapsulated drug for 24 h and 48 h. Increasing concentrations of both free drug and SAHA-encapsulated nanomicelles led to a significant upregulation of p21 ($P<0.05$) and a downregulation of p53 ($P<0.05$) at both 24 h (**Fig. 4a-b)** and 48 h **(Fig. 4d-e)**. Moreover, SAHA loaded nanomicelles were more effective than free SAHA ($P<0.05$) in triggering alterations at the protein level (**Fig. 4a, 4b**), and this effect was corroborated by mRNA expression analysis of the same markers (**Fig. 4c, 4f**), with SAHA loaded nanomicelles having a significantly greater effect on the expression of p21 and p53 mRNA ($P<0.01$) than free drug. The effect of

SAHA and SAHA-loaded nanomicelles on p21 and p53 protein expression appears concentration-dependent, with drug encapsulation potentiating the effect of SAHA in nanomicelles.

The effect of SAHA encapsulation in metastatic processes was also undertaken by determining the expression patterns of E-cadherin and N-cadherin. After 24 h, SAHA and SAHA loaded nanomicelle treatement resulted in a significant upregulation of E-cadherin protein in Hela cells ($P<0.05$) (**Fig. 4c**). Similarly, the 48 h treatment with either SAHA and SAHA nanomicelles resulted in significantly increased E-cadherin expression ($P<0.05$) (**Fig. 4f**). SAHA-encapsulated nanoparticles were more effective than free drug in increasing E-cadherin levels. However, neither SAHA nor SAHA loaded nanomicelles had an effect on N-cadherin expression.

The same analysis was performed on MCF-7 cells, which displayed a similar response to Hela cells after 24 h treatment, with both SAHA and SAHA loaded micelles significantly upregulating p21 and downregulating p53 protein (**Fig. 5a**) and mRNA expression levels (**Fig. 5b**). The same trend was seen after 48 h (**Fig. 5d-e**). Furthermore, SAHA-loaded nanomicelles exhibited a greater effect on protein expression on both targets compared to free SAHA ($P<0.05$). Furthermore, gene expression analysis showed a significant increase in E- cadherin and decrease in N-cadherin after 24 h (**Fig. 5c**), which was maintained after 48 h for E-cadherin only (**Fig. 5f**). In general, SAHA-encapsulated nanoparticles were more effective in increasing the levels of E-cadherins than the free drug.

**Table 1** Characterization of SAHA encapsulated Pluronic nanomicelles. Size, PDI and surface charge were analyzed using Malvern's Zetasizer Nano. Entrapment Efficiency and Drug Loading Efficiency were calculated as explained in **Section 2.2**

| | Size | PDI | Zeta potential | EE% | DL% |
|---|---|---|---|---|---|
| SAHA loaded Pluronic F127 nanomicelles | 22.98±1.01 | 0.08±0.01 | -1.28±0.28 | 94.36±0.76 | 1.31±0.06 |
| Pluronic F127 nanomicelles | 22.56±0.30 | 0.09±0.02 | | | |

# 4. Discussion

Here we have demonstrated that the histone deacetylase inhibitor SAHA can be effectively encapsulated in Pluronic nanoparticles, from which the drug is progressively released for up to 72h. This effect could also be enhanced by the different intracellular uptake patterns of free drugs compared to nano-encapsulated formulations *in vivo*. Indeed, the majority of free drugs enter the cells through a simple diffusion process, while most nanocarrier drugs enter cells through endocytosis [45-47].

As SAHA has been shown to cause harmful side effects on treated patients, analysis of nanomicelle encapsulation was undertaken to evaluate if the drug remained active, as encapsulation could be an

effective route to reducing systemic toxicity. Reported side effects including include fatigue, GI related diarrhea, nausea, thrombocytopenia and anorexia as observed in different types of cancers, including ovarian cancers and lymphomas that have been reported [48, 49]. Experiments on Hela and MCF-7 cells showed that nanomicelle-encapsulated SAHA was in fact more effective than the free drug in causing cell death. This effect was most evident after 72 h, suggesting that drug release a sustained release of SAHA, which would be beneficial in vivo. Furthermore, the encapsulation could result in the use of less drug while still obtaining a therapeutic effect, or in the more effective and tumor site specific delivery due to the inherent properties of nanostructures.

At the molecular level SAHA treatment caused significant changes in proteins involved in both cell cycle and cell phenotype. p53 is plays an important role in many molecular processes including DNA transcription and repair, cell cycle, genomic stability, chromosome segregation, apoptosis, and angiogenesis [50]. p21 is a potent cyclin-dependent kinase inhibitor that can stabilize the interaction between cyclin-dependent kinase (CDK)-4/6 and cyclin D and promote the formation of cyclin D/CDK complexes. Overexpression of p21 leads to the arrest of cells in the G1/G2 or S phases of the cell cycle [21, 51], hence inhibiting the growth of tumor cells [52-54]. Here we demonstrated that SAHA-loaded nanomicelles were able to up-regulate p21 and down-regulate p53 expression, consistent with previous studies on the action of SAHA on tumor growth inhibition by regulating the expression of these genes [36, 38, 39, 55-57].

Detailed analysis of the effects of SAHA-loaded nanoparticles on EMT transition markers revealed a significant upregulated E-cadherin expression, but with no affect N-cadherin expression. This is consistent with previous studies, where HDACi were shown to have only a slight effect on N-cadherin expression in HT-144 and A375 cells [58]. E-cadherins mediate intercellular adhesion through the interaction of the extracellular and cytoplasmic domains with β-catenin. Down-regulation or deletion of E-cadherin expression affects the cadherin-catenin complex formation and stability of the complex, which directly affects the metastatic process [5, 59]. E-cadherin not only enhances cell adhesion but also has anti-proliferative, anti-invasive and anti-metastatic properties [60, 61]. It has been suggested that SAHA may inhibit the formation of Snail and HDAC1/HDAC2 complexes by inhibiting the activity of HDAC1 and HDAC2, leading to the demethylation and transcriptional activation of the E-cadherin. In addition, SAHA may also up-regulate E-cadherin expression by altering its upstream targets (LEF-1 and Slug) [62], but the specific mechanisms need to be further elucidated.

# 5. Conclusions

Encapsulation of SAHA into nanomicelles enhances the potency of this epigenetic drug in breast and cervical cancer cell models. Furthermore this effective formulation will likely enhance drug delivery to tumor sites, and overcome current issues in delivering HDACi to solid tumors, whilst also reducing side effects associated with systemic delivery of the free drug. The enhanced permeability and retention effect (EPR) would enable these nanoparticles to escape via neo-vascularization at tumor sites, and subsequently their physico-chemical characteristics would allow better penetration into solid tumors [63–

66]. Such parameters are likely to be specific to different cancer types, even when just considering Pluronic, where differences in efficacy can be observed [67, 68]. Nanoparticle surface functionalization could be used to further enhance efficacy through the addition of specific moieties that could both enhance delivery to the tumor site, avoiding reliance on the passive EPR uptake effect, and home in on tumor cells overexpressing specific cell surface markers, targeting for example tumor stem cells.

# 6. Declarations

**Competing interests**. The authors declare that they have no competing interests.

**Abbreviations.** EMT: epithelial-to-mesenchymal transition; SAHA: Suberoylanilide Hydroxamic Acid; CTCL: cutaneous T-cell lymphoma; HDAC: histone deacetylase; ROS: reactive oxygen species; TSA: trichostatin A; MDR: multidrug resistance; EPR: enhanced permeability and retention (effect); PEOx-PPOy-PEOz: poly(oxyethylene)-block-poly (oxypropylene)-block-poly(oxyethylene); CPZ: Chlorpromazine; DMSO: Dimethyl sulfoxide; DMEM: Dulbecco's Modified Eagle Medium; PBS: Phosphate buffer solution; PDI: poly-dispersion index; HPLC: High Performance Liquid Chromatography; EE: entrapment efficiency; DL: drug loading (efficiency); CDK: cyclin-dependent kinase; HDACi: Histone deacetylase inhibitors.

**Authors' contributions.** Conceptualization and methodology: CL, RSC and XW; Formal analysis and data curation: SP and XW; Validation and investigation: XW, YH, LH and SP; Writing— original draft preparation and Writing—review and editing: SP, XW, LF, DG, CL and RSC; Approval of final manuscript: all authors. All authors read and approved the final manuscript.

**Funding.** This work was funded by the joint PhD programme Swansea University and Houston Methodist (for SP) and the Welsh National Research Network for Life Science project grant to RSC and CL.

**Availability of data and materials**. The analyzed data sets generated during the present study are available from the corresponding author on reasonable request.

**Acknowledgments**. Not applicable

**Ethics approval and consent to participate.** Not applicable

**Patient consent for publication**. Not applicable

# 7. References

1. Chung S, Yao J, Suyama K, Bajaj, Qian X. Loudig: N-cadherin regulates mammary tumor cell migration through Akt3 suppression. *Oncogene Basingstoke* 2013.
2. Zhu GJ, Song PP, Zhou H, Shen XH, Gao X. Role of epithelial-mesenchymal transition markers E-cadherin, N-cadherin, β-catenin and ZEB2 in laryngeal squamous cell carcinoma. *Oncology Letters* 2018, 15(3).

3. Berndorff D. Liver-intestine cadherin: molecular cloning and characterization of a novel Ca(2+)-dependent cell adhesion molecule expressed in liver and intestine. J Cell Biol. 1994;125(6):1353–69.
4. Yoshida-Noro C, Suzuki N, Takeichi M. Molecular nature of the calcium-dependent cell-cell adhesion system in mouse teratocarcinoma and embryonic cells studied with a monoclonal antibody. Dev Biol. 1984;101(1):19–27.
5. Guo M, Guo M, Mu Y, Mu Y, Yu D, Yu D, Li J, Li J, Chen F, Chen F. Comparison of the expression of TGF–β1, E–cadherin, N–cadherin, TP53, RB1CC1 and HIF–1α in oral squamous cell carcinoma and lymph node metastases of humans and mice. Oncology Letters. 2018;15(2):1639–45.
6. Liu W, Zhang X, Zhao J, Li J, Mao X. Inhibition of cervical cancer cell metastasis by benzothiazole through up-regulation of E-cadherin expression. Microb Pathog. 2017;111:182–6.
7. Zhang F, Ren CC, Liu L, Chen YN, Yang L, Zhang XA, Wang XM, Yu FJ. SHH Gene Silencing Suppresses Epithelial-Mesenchymal Transition, Proliferation, Invasion and Migration of Cervical Cancer Cells by Repressing the Hedgehog Signaling Pathway. *Journal of Cellular Biochemistry* 2017.
8. Gravdal K, Halvorsen OJ, Haukaas SA, Akslen LA. A Switch from E-Cadherin to N-Cadherin Expression Indicates Epithelial to Mesenchymal Transition and Is of Strong and Independent Importance for the Progress of Prostate Cancer. Clinical Cancer Research An Official Journal of the American Association for Cancer Research. 2007;13(23):7003–11.
9. Masoumeh F, Saeed S, Majid FH. Epigenetic mechanisms as a new approach in cancer treatment: An updated review. *Genes & Diseases* 2018:S2352304218300746-.
10. Dupont C, Armant D, Brenner C. Epigenetics: Definition, Mechanisms and Clinical Perspective. Seminars in Reproductive Medicine. 2009;27(05):351–7.
11. Audia JE, Campbell RM. Histone Modifications and Cancer. Cold Spring Harb Perspect Biol. 2016;8(4):a019521.
12. Kawamata N, Chen J, Koeffler HP. Suberoylanilide hydroxamic acid (SAHA; vorinostat) suppresses translation of cyclin D1 in mantle cell lymphoma cells.
13. Prestegui-Martel B, Bermúdez-Lugo JA, Chávez-Blanco A, Due?As-González A, García-Sánchez JR, Pérez-González OA, Padilla-Martínez II, Fragoso-Vázquez MJ, Mendieta-Wejebe JE, Correa-Basurto AM: N-(2-hydroxyphenyl)-2-propylpentanamide, a valproic acid aryl derivative designed\\r < i > in silico\\r with improved anti-proliferative activity in HeLa, rhabdomyosarcoma and breast cancer cells. *J Enzyme Inhib Med Chem* 2016:1–10.
14. Huang L, Pardee AB. Suberoylanilide hydroxamic acid as a potential therapeutic agent for human breast cancer treatment. Mol Med. 2000;6(10):849–66.
15. Kunnimalaiyaan S, Sokolowski K, Gamblin TC, Kunnimalaiyaan M. Suberoylanilide hydroxamic Acid, a histone deacetylase inhibitor, alters multiple signaling pathways in hepatocellular carcinoma cell lines. Am J Surg. 2017;213(4):645–51.
16. Haberland M, Montgomery RL, Olson EN. The many roles of histone deacetylases in development and physiology: implications for disease and therapy. Nat Rev Genet. 2009;10(1):32–42.

17. Xu WS, Parmigiani RB, Marks PA. Histone deacetylase inhibitors: molecular mechanisms of action. Oncogene. 2007;26(37):5541–52.
18. Ververis K, Hiong A, Karagiannis TC, Licciardi PV. Histone deacetylase inhibitors (HDACIs): multitargeted anticancer agents. Biologics Targets Therapy. 2013;7(default):47–60.
19. Bolden JE, Peart MJ, Johnstone RW. Anticancer activities of histone deacetylase inhibitors. Nat Rev Drug Discovery. 2006;5(9):769–84.
20. Lindemann RK, Gabrielli B, Johnstone RW. Histone-Deacetylase Inhibitors for the Treatment of Cancer. Cell Cycle. 2004;3(6):777–86.
21. Zhang J, Zhong Q. Histone deacetylase inhibitors and cell death. Cellular Molecular Life Sciences. 2014;71(20):3885–901.
22. Alexander NR, Tran NL, Rekapally H, Summers CE, Glackin C, Heimark RL. N-cadherin Gene Expression in Prostate Carcinoma Is Modulated by Integrin-Dependent Nuclear Translocation of Twist1. Can Res. 2006;66(7):3365–9.
23. Gloushankova NA, Rubtsova SN, Zhitnyak IY. Cadherin-mediated cell-cell interactions in normal and cancer cells. *Tissue Barriers* 2017:e1356900.
24. Nagaraj N. Pierre, Massion, Adriana, Gonzalez, Pengcheng: Smoking induces epithelial-to-mesenchymal transition in non-small cell lung cancer through HDAC-mediated downregulation of E-cadherin. *Molecular Cancer Therapeutics* 2012.
25. Friedl P, Locker J, Sahai E, Segall JE. Classifying collective cancer cell invasion. Nat Cell Biol. 2012;14(8):777–83.
26. Bravo-Cordero JJ, Hodgson L, Condeelis J. Directed cell invasion and migration during metastasis. Curr Opin Cell Biol. 2012;24(2):277–83.
27. Konsoula R, Jung M. In vitro plasma stability, permeability and solubility of mercaptoacetamide histone deacetylase inhibitors. Int J Pharm. 2008;361(1–2):19–25.
28. Qi SS, Sun JH, Yu HH, Yu SQ. Co-delivery nanoparticles of anti-cancer drugs for improving chemotherapy efficacy. Drug Delivery. 2017;24(1):1909–26.
29. Papahadjopoulos D, Allen TM, Gabizon A, Mayhew E, Matthay K, Huang SK, Lee KD, Woodle MC, Lasic DD, Redemann C. Sterically stabilised liposomes: improvements in pharmacokinetics and anti-tumour therapeutic efficacy. 1991.
30. Tsutsui Y, Tomizawa K, Nagita M, Michiue H, Nishiki TI, Ohmori I, Seno M, Matsui H. Development of bionanocapsules targeting brain tumors. J Controlled Release. 2007;122(2):159–64.
31. Soppimath KS, Aminabhavi TM, Kulkarni AR, Rudzinski WE. Biodegradable polymeric nanoparticles as drug delivery devices. J Controlled Release. 2001;70(1–2):1.
32. Janes KA, Fresneau MP, Marazuela A, Fabra A. Alonso MaJ: Chitosan Nanoparticles as Delivery Systems for Doxorubicin. J Controlled Release. 2001;73(2–3):255–67.
33. Ai H, Khemtong C, Guthi JS, Chin SF, Sherry AD, Boothman DA, Gao J, Nasongkla N, Bey E, Ren J. Multifunctional Polymeric Micelles as Cancer-Targeted, MRI-Ultrasensitive Drug Delivery Systems.

Nano Lett. 2006;6(11):2427–30.

34. Zhu Y, Liao L. Applications of Nanoparticles for Anticancer Drug Delivery: A Review. Journal of Nanoscience Nanotechnology. 2015;15(7):4753–73.
35. Zhu P, Zhao N, Sheng D, Hou J, Hao C, Yang X, Zhu B, Zhang S, Han Z, Wei L. Inhibition of Growth and Metastasis of Colon Cancer by Delivering 5-Fluorouracil-loaded Pluronic P85 Copolymer Micelles. Sci Rep. 2016;6(1):20896.
36. Russo A, Pellosi DS, Pagliara V, Milone MR, Pucci B, Caetano W, Hioka N, Budillon A, Ungaro F, Russo G. Biotin-targeted Pluronic? P123/F127 mixed micelles delivering niclosamide: A repositioning strategy to treat drug-resistant lung cancer cells. Int J Pharm. 2016;511(1):127–39.
37. Fang J, Nakamura H, Maeda H. The EPR effect: Unique features of tumor blood vessels for drug delivery, factors involved, and limitations and augmentation of the effect. Adv Drug Deliv Rev. 2010;63(3):136–51.
38. Antitumor activity. of vorinostat-incorporated nanoparticles against human cholangiocarcinoma cells. Journal of Nanobiotechnology. 2015;13(1):60.
39. Tran TH, Choi JY, Ramasamy T, Truong DH, Nguyen CN, Choi HG, Yong CS, Kim JO. Hyaluronic acid-coated solid lipid nanoparticles for targeted delivery of vorinostat to CD44 overexpressing cancer cells. Carbohyd Polym. 2014;114:407–15.
40. Biswas S, Vaze OS, Movassaghian S, Torchilin VP: Polymeric Micelles for the Delivery of Poorly Soluble Drugs: John Wiley & Sons Ltd; 2013.
41. Farrugia M, Morgan SP, Alexander C, Mather ML. Ultrasonic monitoring of drug loaded Pluronic F127 micellular hydrogel phase behaviour. Materials Science Engineering C Materials for Biological Applications. 2014;34:280–6.
42. De Mello JC, Moraes VW, Watashi CM, Silva DC, Cavalcanti LP, Franco MK, Yokaichiya F, Araujo DR, Rodrigues T. Enhancement of chlorpromazine antitumor activity by Pluronics F127/L81 nanostructured system against human multidrug resistant leukemia. *Pharmacological Research* 2016:S1043661816305266.
43. Zhang D, Tao L, Zhao H, Yuan H, Lan M. A functional drug delivery platform for targeting and imaging cancer cells based on Pluronic F127. Journal of Biomaterials Science Polymer Edition. 2015;26(8):468–82.
44. Zeng Z, Peng Z, Chen L, Chen Y. Facile fabrication of thermally responsive Pluronic F127-based nanocapsules for controlled release of doxorubicin hydrochloride. Colloid Polymer Science. 2014;292(7):1521–30.
45. Kumari P, Swami MO, Nadipalli SK, Myneni S, Ghosh B, Biswas S. Curcumin Delivery by Poly(Lactide)-Based Co-Polymeric Micelles: AnIn VitroAnticancer Study. Pharm Res. 2016;33(4):826–41.
46. Parisa F. Azlan, Abdul, Aziz: Insight into Cellular Uptake and Intracellular Trafficking of Nanoparticles. *Nanoscale research letters* 2018.

47. Behzadi S, Serpooshan V, Tao W, Hamaly MA, Alkawareek MY, Dreaden EC, Brown D, Alkilany AM, Farokhzad OC, Mahmoudi M. Cellular uptake of nanoparticles: journey inside the cell. Chem Soc Rev. 2017;46(14):4218–44.
48. Duvic M. Histone deacetylase inhibitors: SAHA (Vorinostat). A treatment option for advanced cutaneous T-cell lymphoma. *Hematology Meeting Reports* 2009.
49. Noriyuki T. Hisashi, Narahara: Histone deacetylase inhibitor therapy in epithelial ovarian cancer. *Journal of Oncology* 2010.
50. Xu B, Li M, Yu Y, He J, Hu S, Pan M, Lu S, Liao K, Pan Z, Zhou Y. Effects of harmaline on cell growth of human liver cancer through the p53/p21 and Fas/FasL signaling pathways. *Oncology Letters* 2017.
51. Li LH, Zhang PR, Cai PY, Li ZC. Histone deacetylase inhibitor, Romidepsin (FK228) inhibits endometrial cancer cell growth through augmentation of p53-p21 pathway. Biomed Pharmacother. 2016;82:161–6.
52. Karam JA, Fan J, Stanfield J, Richer E, Benaim EA, Frenkel E, Antich P, Sagalowsky AI, Mason RP, Hsieh JT. The use of histone deacetylase inhibitor FK228 and DNA hypomethylation agent 5-azacytidine in human bladder cancer therapy. Int J Cancer. 2007;120(8):1795–802.
53. Liu H, Luo Q, Cui H, Deng H, Zhao L. Sodium fluoride causes hepatocellular S-phase arrest by activating ATM-p53-p21 and ATR-Chk1-Cdc25A pathways in mice. Oncotarget. 2017;9(4):4318–37.
54. Seta T, Imazeki F, Yokosuka O, Saisho H, Isono K. Expression of p53 and p21WAF1/CIP1 Proteins in Gastric and Esophageal Cancers (Comparison with Mutations of the p53 Gene). Digestive Diseases Sciences. 1998;43(2):279–89.
55. Davies C, Hogarth LA, Mackenzie KL, Hall AG, Lock RB. P21WAF1 modulates drug-induced apoptosis and cell cycle arrest in B-cell precursor acute lymphoblastic leukemia. *Cell Cycle* 2015, 14(22).
56. Ogata T, Nakamura M, Sang M, Yoda H, Ozaki T. Depletion of runt-related transcription factor 2 (RUNX2) enhances SAHA sensitivity of p53-mutated pancreatic cancer cells through the regulation of mutant p53 and TAp63. Plos One. 2017;12(7):e0179884.
57. Zhou H, Cai Y, Liu D, Li M, Sha Y, Zhang W, Wang K, Gong J, Tang N, Huang A: Pharmacological or transcriptional inhibition of both HDAC1 and 2 leads to cell cycle blockage and apoptosis via p21 < sup > Waf1/Cip1</sup > and p19 < sup > INK4d</sup > upregulation in hepatocellular carcinoma. *Cell Proliferation* 2018:e12447.
58. Díaz-Nú?Ez M, Díez-Torre A, De Wever O, Andrade R, Arluzea J, Silió M, Aréchaga J. Histone deacetylase inhibitors induce invasion of human melanoma cells in vitro via differential regulation of N-cadherin expression and RhoA activity. 2016.
59. Zhang ZY, Wu YQ, Zhang WG, Tian Z, Cao J. The expression of E-cadherin-catenin complex in adenoid cystic carcinoma of salivary glands. Chinese Journal of Dental Research the Official Journal of the Scientific. 2000;3(3):36–9.
60. Balaram P, Alex S, Panikkar B, Rajalekshmi TN. Adhesion-related proteins E-cadherin, P-cadherin, CD44, and CD44v6, and antimetastatic protein nm23H1 in complete hydatidiform moles in relation

to invasion potential. Int J Gynecol Cancer. 2004;14(3):532–9.

61. Kilgore J, Jackson AL, Clark LH, Guo H, Zhang L, Jones HM, Gilliam TP, Gehrig PA, Zhou C, Baejump VL. Buformin exhibits anti-proliferative and anti-invasive effects in endometrial cancer cells. American Journal of Translational Research. 2016;8(6):2705.
62. Dara N, Tang SN, Marianna R, Srivastava RK, Sharmila S, Batra SK. Targeting Epigenetic Regulation of miR-34a for Treatment of Pancreatic Cancer by Inhibition of Pancreatic Cancer Stem Cells. Plos One. 2011;6(8):e24099-.
63. Torchilin V. Tumor delivery of macromolecular drugs based on the EPR effect. Adv Drug Deliv Rev. 2011;63(3):131–5.
64. Maeda H, Wu J, Sawa T, Matsumura Y, Hori K. Tumor vascular permeability and the EPR effect in macromolecular therapeutics: a review. 2000, 65(1–2):271–284.
65. Blanco E, Shen H, Ferrari M. Principles of nanoparticle design for overcoming biological barriers to drug delivery. Nat Biotechnol. 2015;33(9):941.
66. Zhang YR, Lin R, Li HJ, He WL, Du JZ, Wang J. Strategies to improve tumor penetration of nanomedicines through nanoparticle design. *Wiley Interdisciplinary Reviews Nanomedicine & Nanobiotechnology* 2018:e1519.
67. Xu J, Sun J, Wang P, Ma X, Li S. Pendant HDAC Inhibitor SAHA Derivatized Polymer as a Novel Prodrug Micellar Carrier for Anticancer Drugs. *Journal of Drug Targeting* 2017:1–32.
68. Ghanta P, Ghosh, Balaram, Biswas, Swati, Trivedi, Prakruti, Kumari, Preeti: Polymeric micelles of suberoylanilide hydroxamic acid to enhance the anticancer potential in vitro and in vivo. *Nanomedicine* 2017.

# Figures

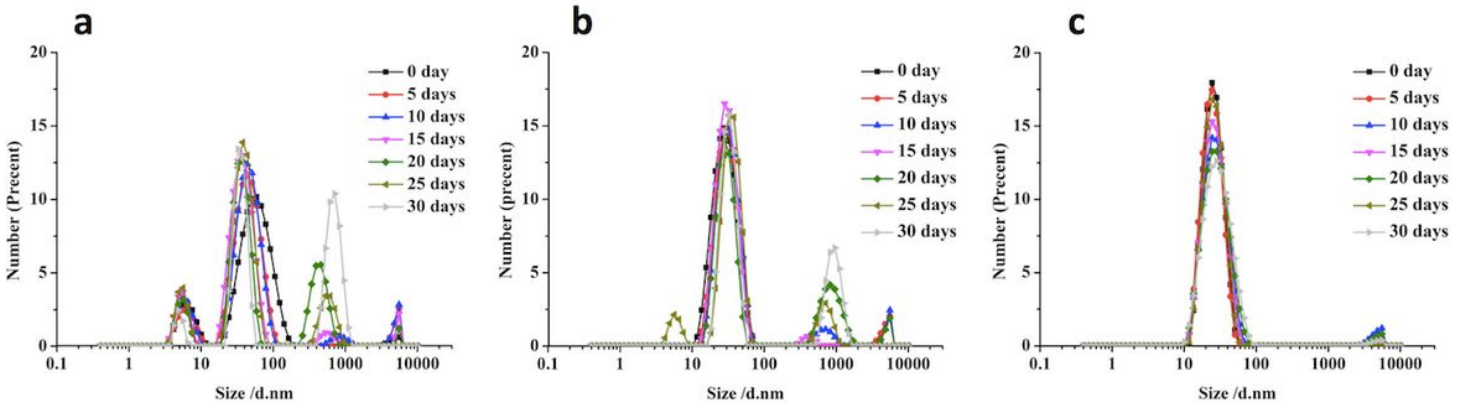


**Figure 1**

Analysis of nanoparticles stability over time. The aggregation of nanomicelles in three different solvents was investigated at 0,5,10,15,20,25 and 30 days. Nanoparticles were kept at 4°C. 1a H2O; 1b 10 mM PBS; 1c 150 mM PBS

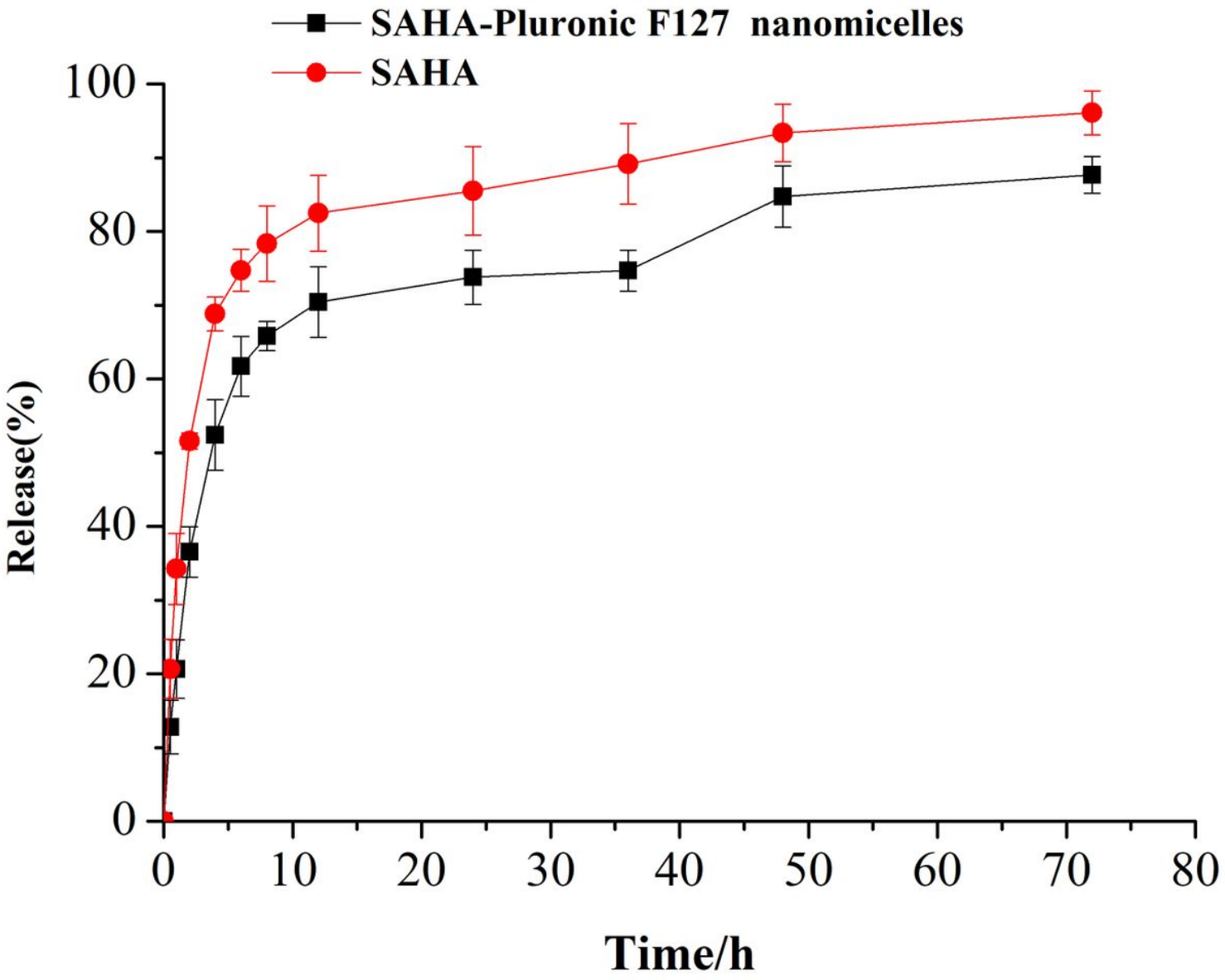


**Figure 2**

In vitro drug release of SAHA from nanomicelles. Nanomicelles encapsulated with SAHA and resuspended in PBS were tested for their capacity to release the drug over time. HPLC was used to measure the amount of SAHA released after up to 72 h. The ±SD value of the data was tested by T test (n=3).

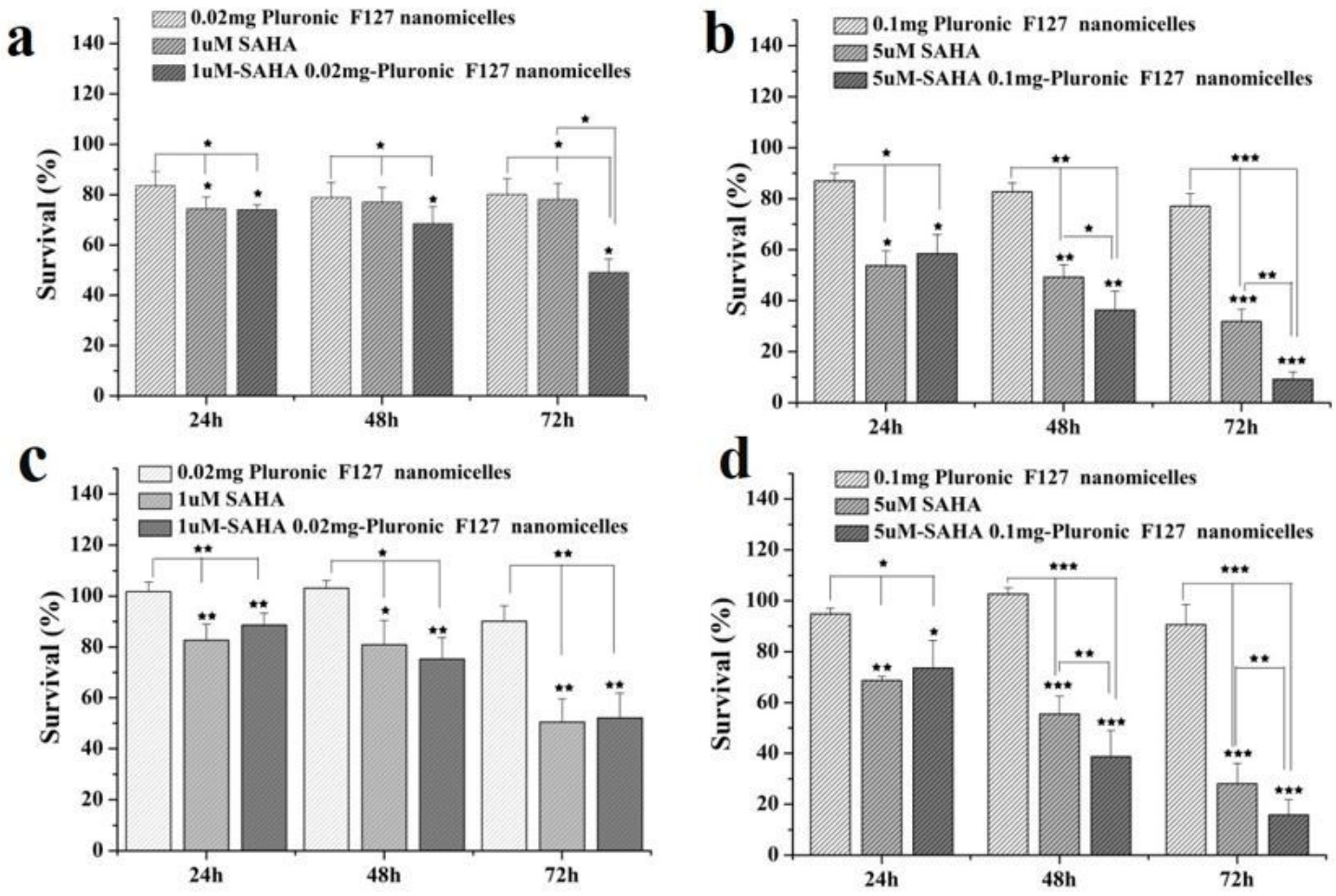


## Figure 3

Anti-proliferative effect of SAHA on Hela and MCF-7 cells. 3a, 3b effect of different drug concentrations on Hela cells at 24 h, 48 h and 72 h. 3c, effect of different drug concentrations on MCF-7 cells. Survival rate was measured by MTT assay. The percentage of viable cells was determined as the ratio of treated cells to untreated controls. A one-way ANOVA was used to test for statistical significance (*P<0.05, **P<0.01, ***P<0.001).

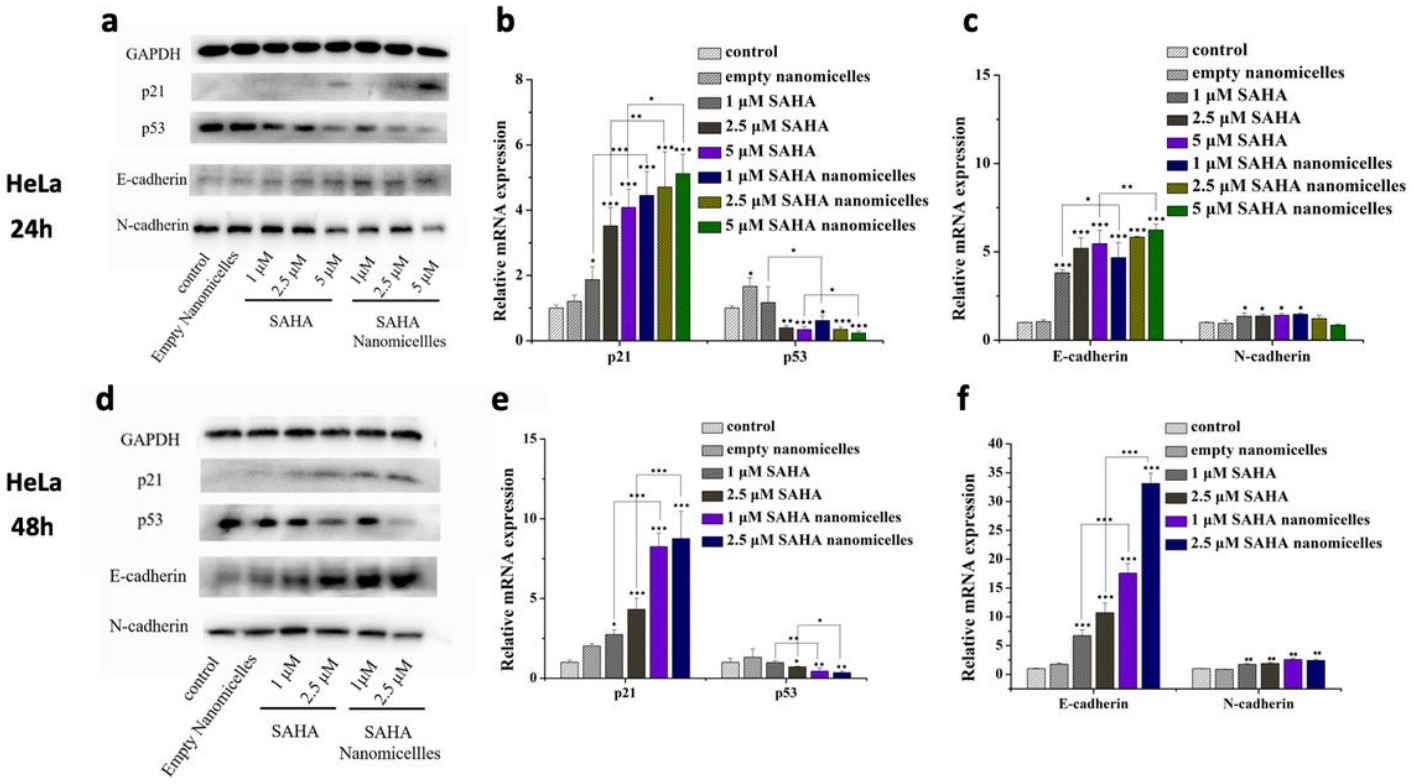


## Figure 4

Protein and mRNA expression of p21, p53, E/N-cadherins in Hela cells after 24 (top) or 48 hours (bottom). Cells were analyzed by western blot and qPCR. 4a, 4d Effect of SAHA and SAHA loaded nanomicelles on the protein expression of the four markers in Hela cells at 24 and 48 h. 4b, 4e mRNA analysis of p21 and p53 markers on Hela cells at 24 and 48 h. 4c, 4f Effect of SAHA and SAHA loaded nanomicelles on E and N-cadherin mRNA expression in Hela cells at both time points. Data were normalized to the level of GAPDH. Data were tested by T test for statistical significance (n=3, *P<0.05, **P<0.01, ***P<0.001).

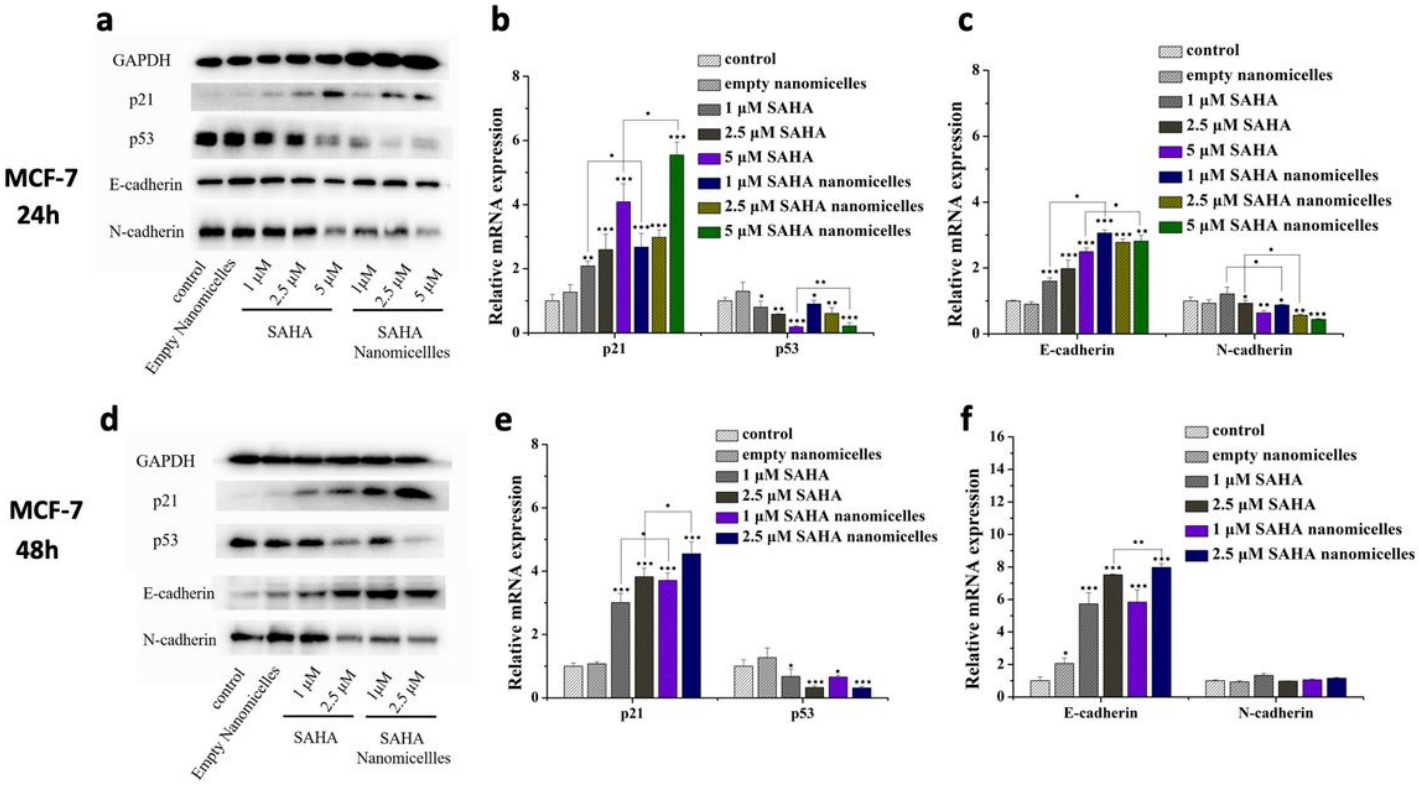


## Figure 5

Protein and mRNA expression of p21 and p53 in MCF-7 cells after 24 (top) or 48 hours (bottom). The effect of SAHA and SAHA loaded nanomicelles on p53 and p21 protein expression in MCF-7 cells was analyzed. Expression of all four markers was analyzed by western blot at 24 (5a) and 48 h (5d). Data were normalized to the level of GAPDH. The effect of SAHA and SAHA loaded nanomicelles on p21 and p53 mRNA expression was also done at 24 h (5b) and 48 h (5e), and normalized to the level of GAPDH, while the E- and N-cadherin mRNA analysis at 24 and 48 h is shown in (5c) and (5f), respectively. The expression level is shown relative to the control as 1. A t-test to test for statistical significance was performed (*P<0.05, **P<0.01, ***P<0.001)